Surface Barriers of Hydrocarbon Transport Triggered by Ideal Zeolite Structures

Nils E. R. Zimmermann,[*,†] Sayee P. Balaji,[†,‡] and Frerich J. Keil[†]

Chemical Reaction Engineering, Hamburg University of Technology, Eissendorfer Str. 38, 21073 Hamburg, Germany

E-mail: nils.zimmermann@tu-harburg.de

[†]Hamburg University of Technology

[‡]Current address: Process & Energy Laboratory, Delft University of Technology, Leeghwaterstraat 44, 2628 CA Delft, The Netherlands

Abstract

Shedding light on the nature of surface barriers of nanoporous materials, molecular simulations (Monte Carlo, Reactive Flux) have been employed to investigate the tracer-exchange characteristics of hydrocarbons in defect-free single-crystal zeolite membranes. The concept of a critical membrane thickness as quantitative measure of surface barriers is shown to be appropriate and advantageous. Nanopore smoothness, framework density, and thermodynamic state of the fluid phase have been identified as the most important influencing variables of surface barriers. Despite the ideal character of the adsorbent, our simulation results clearly support current experimental findings on MOF Zn (tbip) where a larger number of crystal defects caused exceptionally strong surface barriers. Most significantly, our study predicts that the ideal crystal structure without any such defects will already be a critical aspect of experimental analysis and process design in many cases of the upcoming class of extremely thin and highly oriented nanoporous membranes.

Keywords: boundary layer, nanoporous, diffusion, tracer-exchange, TST.

Introduction

The current prospect of increasing usage of fossil fuels in conjunction with the ongoing research on carbon dioxide sequestration excites interest in processes employing nanoporous materials as catalyst or separation medium in order to open alternative routes to existing technologies. Carbon nanotubes (CNTs), metal-organic frameworks (MOFs) and zeolites represent the foremost candidates to be incorporated in such applications.[1–6] An integral part of the process design will be the role of transport of the guest molecules into, through and out of the nanopores.[5–10]

Recent progress in the synthesis of zeolite membranes[10] paves the way for ultra-thin films which may be used on a support layer as molecular sieve membranes with low internal transport resistance. In such cases, however, the issue of surface barriers, i.e. transport resistances located in the boundary layer between intracrystalline space and fluid phase, arises because these barriers may dominate the overall transport for very thin membranes (or crystals).[7,8,11] In this context, two aspects are important:

1. Approximately, up to which membrane thickness or crystal size, respectively, will the influence of surface barriers be noticeable?

2. What do those barriers depend on? And, what triggers them?

To address the above questions, the influences of molecule type and chain length of normal hydrocarbons (C1-C6) as well as the temperature, and the impact of the nanopore structure on surface barriers in all-silica zeolites of topologies AFI, LTL and MFI are investigated in this study. State-of-the-art molecular simulation approaches are employed on ideal systems, and the previously proposed criterion of a critical membrane thickness,[8] δ_{crit}, serves as a quantitative measure of surface barriers.

Methodology

For the sake of brevity and because most of the methodology was adopted from our previous work,[8] this section focuses on the zeolite structures studied and reiterates the concept of a critical membrane thickness as an assessment of surface barriers[8,11] (question one from the Introduction). In short however, the framework of dynamically corrected transition state theory was employed where Monte Carlo simulations in the NVT ensemble (NVT-MC) provided residence histograms of the guest molecules [$P(q)$], and reactive flux simulations yielded transmission coefficients (κ) of the elementary transport processes identified. On this basis, molar fluxes at the barriers considered were computed. More simulation details are available in the Supporting Information (Section 1).

Zeolites

Two zeolite structures featuring one-dimensional pore systems (AFI, LTL) and a structure with a 3D pore network (MFI) were studied whereby all zeolites were purely siliceous (SiO_2). The major difference between the AFI and the LTL structure is the larger cage-to-window ratio of the latter. Within the categorization of Ref. 12, all three types of nanopores and diffusion behaviors are hence investigated: channel-type (AFI), cage-type (LTL) and intersecting channel-type (MFI). The crystal structures were taken from Ref. 13–15 and, if necessary, converted to purely siliceous structures.[16] The AFI and LTL unit cells accommodate in total four and two cages, respectively, whereas four intersections of straight (y direction) and zigzag (x-z) channels are found in a single MFI unit cell (Figure 1). The zeolite atoms were kept fixed at their crystallographic positions because framework flexibility in the sense of a dynamic effect (e.g. breathing window) does not have any significant influence on adsorption and diffusion in zeolites.[17] However, diffusion coefficients may be quite sensitive to subtle differences in the time-averaged crystal structure in consequence of a flexible zeolite lattice[16,18,19] for which reason the rigid-lattice assumption used in this work seems to be justified.[17]

As in our previous study, the zeolite crystal slabs consisted of full unit cells and fractional,

concluding unit cells at the outer surface, and the slabs were centered in the simulation box. In each case two different external surfaces were investigated. The AFI and LTL pores were cut such to let the pore windows (left) and cages (right) terminate the pores which run along the z direction (Figure 1 top and center). As for MFI, the single-crystal membrane was aligned along the straight channels (y direction), because the flux is maximal in this direction.[1,7] The MFI unit cells were cut at fractional coordinates of 0.125 and 0.73. This yielded a left surface that exhibits tighter "canyons" for guest molecules to enter the zeolite in comparison to the right surface which is rather flat giving quite direct access to the straight channels (Figure 1 bottom).

Free-energy profiles are plotted along with the respective pore structure in Figure 1. They indicate that adsorbate molecules "feel" the internal channel structure being not affected by the presence of the external surface. Therefore, the computation of a single representative flux ($j^{\ddagger}_{\mathrm{zeol}}$) between the innermost adsorption sites/cages, i.e. through the dividing surface $q^{\ddagger}_{\mathrm{zeol}}$, as indicated in Figure 1, is justified for the bulk zeolite fluxes. The environment inside the cage or intersection next to the surface, i.e. where the flux $j^{\ddagger}_{\mathrm{surf}}$ prevails, is slightly different from the innermost cages; particularly for the side towards the pore mouth. Thus, on a microscopic scale, the single-crystal membrane is composed of two types of regions, each with its characteristic flux:

1. The innermost cages/intersections which are assembled to an n_{s}-long array of consecutive slabs, making up the largest part of the membrane, see also Supporting Figure 3. The equilibrium flux $j^{\ddagger}_{\mathrm{zeol}}$ establishes between two adjacent "cage" slabs.

2. The cages/intersections next to the pore mouth (surface) where $j^{\ddagger}_{\mathrm{surf}}$ establishes between this first slab and the external surface adsorption layer.

Assessment of Surface Barriers

The problem arising with the assumption of zero surface barriers may be demonstrated, in a descriptive way, by mimicking a tracer-exchange experiment.

It is straightforward to compute relative exchange curves, $M(t)/M_{\infty}$, on the basis of the fluxes

(Supporting Section 1.3). An often employed procedure to evaluate such curves is given in Ref. 20 (§4.3.2):

$$\frac{M(t)}{M_\infty} = 1 - \sum_{i=0}^{\infty} \frac{8 \cdot \exp[-D_{\mathrm{S,eff}}(2i+1)^2\pi^2 t/\delta^2]}{(2i+1)^2\pi^2}, \tag{1}$$

where $D_{\mathrm{S,eff}}$ denotes the (effective) self-diffusion coefficient, t the time and δ the membrane thickness. This procedure assumes no transport barrier be present in the zeolite boundary layer. Meanwhile, the ansatz $j^{\ddagger}_{\mathrm{surf}}(t) = \alpha[c_{\mathrm{surf},\infty} - c_{\mathrm{surf}}(t)]$, with $c_{\mathrm{surf},\infty}$ the equilibrium surface concentration of labeled molecules, leads to an alternative model that accounts for surface barriers (cf. §4.3.6 in Ref. 20):

$$\frac{M(t)}{M_\infty} = 1 - \sum_{i=1}^{\infty} \frac{2L^2 \exp[-\gamma_i^2 D_{\mathrm{S}} t/(\delta/2)^2]}{\gamma_i^2(\gamma_i^2 + L^2 + L)}, \tag{2}$$

with D_{S} the (true) self-diffusion coefficient and $L = (\delta/2)\alpha/D_{\mathrm{S}}$; γ_i are the positive roots of $\gamma_i \tan\gamma_i = L$. The surface permeability, α, is a measure for the mass transport rate at the surface. The smaller the permeability, the larger will be the surface barrier. Because of the lack of a permeability in the first procedure, the diffusion coefficient will be an effective value, $D_{\mathrm{S,eff}}$, that comprises both the intracrystalline transport resistance plus the surface resistance. As a result, the effective diffusivity, $D_{\mathrm{S,eff}}$, increases with membrane thickness, see Figure 2 (filled circles). By contrast, the diffusivity obtained with the second model, D_{S}, remains constant over δ (squares in Figure 2) and it equals the theoretical estimate by dynamically corrected transition state theory,[21] $D_{\mathrm{S}}^{\mathrm{dcTST}}$ (dotted line). The first procedure is in widespread use for the evaluation of uptake experiments by, for example, gravimetric measurements. Therefore, the difference between the effective and the true diffusion coefficient can be used as a measure of the surface barrier because it rates the incorporation of an error due to the inadequate use of the no-surface-barrier boundary condition.

The main message of Figure 2 is that there exists a certain membrane thickness for which surface barriers are insignificant because $D_{\mathrm{S,eff}}$ and D_{S} are similar for this thickness and all larger ones. To calculate an estimate of this thickness, δ_{crit}, on the basis of molecular simulation data, we

have introduced a simple criterion in Ref. 8:

$$\delta_{\mathrm{crit}} = 2 \cdot \frac{j^{\ddagger}_{\mathrm{zeol}}}{j^{\ddagger}_{\mathrm{surf}}/\lambda}, \tag{3}$$

where λ denotes the cage and intersection separation, respectively, i.e. the characteristic length of a single diffusion event. As can be seen from Figure 2 and Supporting Figure 5, the effective self-diffusivity will always be a factor of 3.6 to 4.5 smaller than the true one, as far as a membrane of δ_{crit} thickness is considered. Hence, surface barriers are of considerable magnitude for membranes of thickness δ_{crit} and smaller, but negligible for thicker ones. Note that the above equation differs from our previous definition in Ref. 8 to enable a direct comparison to Ref. 9, where instead of $j^{\ddagger}_{\mathrm{zeol}}/j^{\ddagger}_{\mathrm{surf}}$ the ratio between the surface permeability, α, and diffusivity, D_{S}, have been employed to assess surface barriers, because $j^{\ddagger}_{\mathrm{zeol}} \propto D_{\mathrm{S}}$ and $j^{\ddagger}_{\mathrm{surf}} \propto \alpha$.

Results

We will now, on the basis of our simulation results, address to the second question from the Introduction, i.e. what surface barriers depend on. Note that the temperatures in the simulations were set to $T = 1.05 \cdot T_{\mathrm{crit}}$, with T_{crit} the guest molecule's critical temperature,[22] to ensure similar corresponding states for the investigation of chain length and pore structure influence. The force field developed by Dubbeldam et al.[23] and extended by Liu et al.[24] was used with some minor differences (Supporting Section 1.2).

One-Dimensional Pores

The critical membrane thicknesses of *n*-alkanes and *n*-alkenes adsorbed in all-silica AFI single-crystal membranes decrease with increasing pressure (Figure 3). Surface barriers will therefore have a profound impact on the overall tracer-exchange process for a wider range of membrane thicknesses at low pressures as compared to high *p*. This observation is consistent with previ-

ous results[8] and underlines that this behavior is quite general irrespective of the guest molecule, the nature of the external crystal surface and the host material as such (Figure 4 and Figure 5). Comparing the simulation results (symbols in Figure 3) with predictions[8] (lines) where the surface flux is substituted for by the mean flux in the gas phase ($j^{\ddagger}_{\mathrm{surf}} \rightarrow j_{\mathrm{gas}}$), the model reliably predicts the trend and in most cases even the magnitude of the critical thickness up to pressures of about $p^* = 0.1$.

A common trend can be observed from Figure 3. As the thermodynamical critical point at $p^* = 1$ is approached, the magnitude of the critical thickness, δ_{crit}, becomes comparable to the size of the unit cell. Surface barriers do thus not matter for any membrane width, as long as the fluid phase is near-critical. On the other extreme, the trend of δ_{crit} signifies that the more the fluid phase behaves like an ideal gas (left-hand side), the stronger will be the impact of the surface barriers. Inserting a single molecule into the simulation box ($p^* \rightarrow 0$) maximizes therefore the critical membrane thickness for a given host-guest system (left end of abscissa). The value of δ_{crit} obtained at the smallest finite pressure for a given fluid is already close to this maximum. It thus starts decreasing significantly when the isotherm *increases* distinctly (Supporting Figure 6).

At equal reduced pressures, an increase of δ_{crit} with molecule chain length is appreciable – particularly in the zero-pressure limit. In contrast to the chain length, the type of molecule – alkane *vs.* alkene – does not reveal such a clear trend. Therefore, one might state that the molecule type has a weaker impact than the chain length because the critical thicknesses for comparable chain molecules, i.e. ethane *vs.* ethene and propane *vs.* propene, respectively, are more similar as compared with the next larger chain molecule, i.e. propane/propene *vs.* butane. Considering the error bars and the moderate spread of the critical thicknesses at equal pressures leads to the conclusion that even the hydrocarbon chain length has a rather small influence and levels off, the longer the chain becomes. Finally, the nature of the surface (cage *vs.* window-wise truncated membrane side) does not have any influence on the critical AFI thickness at all (cf. Supporting Figure 9).

As for LTL, similar trends can be observed (Figure 4), with two exceptions. First, the critical

membrane thickness is quite constant for the C1 and C2 chains so that a distinct decrease over pressure is only appreciable for the longer chains. And second, the LTL surface itself seems to have some influence on the critical thickness (cf. Supporting Figure 10).

The two most striking facts about the LTL results are that the critical thicknesses are roughly one order of magnitude smaller than the AFI values, and they are, for most pressures, close to the theoretical lower limit of the membrane size (z_{UC}). At this point, it is instructive to turn the attention back to the free-energy profiles of Figure 1. These profiles, obtained from simulations with a single methane molecule, give a good impression of how far δ_{crit} will be apart from this lower membrane limit. If the free energy of the barrier at the external surface, $F(q^{\ddagger}_{\mathrm{surf}}) = F^{\ddagger}_{\mathrm{surf}}$, is similar to the one within the (repetitive) intracrystalline space (i.e. $F^{\ddagger}_{\mathrm{surf}} \sim F^{\ddagger}_{\mathrm{zeol}}$), δ_{crit} will be close to the lower limit. This is true for LTL but not for AFI where the $F^{\ddagger}_{\mathrm{zeol}}$ is markedly smaller than $F^{\ddagger}_{\mathrm{surf}}$. It is intuitive altogether that relatively large intracrystalline diffusion barriers render the associated surface barriers less significant.

Intersecting Channels

Figure 5 summarizes the results obtained with the MFI-type membranes. Because the MFI slabs were aligned along the maximal flux direction,[7] the worst case for the surface barriers is probed. Investigating MFI membranes along the *x* or *z* coordinate will result in smaller critical membrane thicknesses. Large error bars in the butane and hexane data at the right boundary layer (Figure 5b) are observed because vanishing entrance barriers have led to overly sensitive transmission coefficients (cf. Figure 1, blue rectangle). A twofold increase in reactive flux trajectories from 5,000 to 10,000 did not improve the statistical accuracy, as expected.[25]

The critical membrane thicknesses in Figure 5a (i.e. obtained with the left surface flux) follow a common trend line, irrespective of the molecule type. Taking into account the high uncertainties of δ_{crit} at the right surface, it may be concluded that the trend-line collapse is even independent of the surface nature. It thus resembles the "LTL behavior" of δ_{crit} (high diffusion barrier). On the other hand, the magnitude of δ_{crit} is comparable to the AFI data (low ΔF_{zeol}). Hence, both large

surface and large intracrystalline diffusion barriers can be observed for MFI.

The magnitude of the critical thickness in MFI-membranes is strikingly sensitive to the truncation plane of the crystal membrane. This is in agreement with the findings by García-Pérez et al.[26] who investigated ethane-propane adsorption on silicalite-1 surfaces. The authors observed that the surface excess adsorption was dependent on where the crystal was truncated. As can be seen from Figure 1 bottom, "canyons" form the entrance to the MFI pore network on either side of the crystal slab. The left-hand canyons are however evidently tighter, providing indication for an increasing steric hindrance to pore entrance at the left boundary layer as the molecule chain grows.

Temperature

Considering the example of the hydrocarbon-AFI systems, the influence of temperature on surface barriers was investigated. The zero-pressure regime is considered only to probe the case of maximal impact of the surface barriers, and it is assumed that the ratio of transmission coefficients ($\kappa_{\mathrm{zeol}}/\kappa_{\mathrm{surf}}$) remains constant with varying temperature (Supporting Table 3).

Defining $T_{\mathrm{ref}} \equiv 1.05 \cdot T_{\mathrm{crit}}$, the ratio of the critical membrane thickness at any temperature relative to the one at the reference temperature (i.e. the enhancement) reduces to

$$\frac{\delta_{\mathrm{crit}}(T)}{\delta_{\mathrm{crit}}(T_{\mathrm{ref}})} = \frac{P^{\ddagger}_{\mathrm{zeol}}(T)/P^{\ddagger}_{\mathrm{surf}}(T)}{P^{\ddagger}_{\mathrm{zeol}}(T_{\mathrm{ref}})/P^{\ddagger}_{\mathrm{surf}}(T_{\mathrm{ref}})} = \frac{\exp\left\{\beta\left[F^{\ddagger}_{\mathrm{surf}}(T) - F^{\ddagger}_{\mathrm{zeol}}(T)\right]\right\}}{\exp\left\{\beta_{\mathrm{ref}}\left[F^{\ddagger}_{\mathrm{surf}}(T_{\mathrm{ref}}) - F^{\ddagger}_{\mathrm{zeol}}(T_{\mathrm{ref}})\right]\right\}} \tag{4}$$

with $P^{\ddagger}_{i}$ denoting the residence probability at the barrier (‡) i. Instead of correlating this enhancement directly with the corresponding temperature variation (i.e. T/T_{ref}), the abscissa in Figure 6, which depicts the results, is the square root of a dimensionless coefficient X. This coefficient is defined as

$$X \equiv \exp\left[\frac{a \cdot n + \Delta H_{\mathrm{ads},0}}{R} \cdot \left(\frac{1}{T} - \frac{1}{T_{\mathrm{ref}}}\right)\right], \tag{5}$$

where R denotes the universal gas constant and a and $\Delta H_{\mathrm{ads},0}$ are parameters that describe the linear relationship between molecular chain length, n, and heat of adsorption, ΔH_{ads}. From the defini-

tion of X follows that it effectively represents the enhancement of the Henry coefficient induced by temperature reduction[27] [i.e. $K_{\mathrm{H}}(T)/K_{\mathrm{H}}(T_{\mathrm{ref}})$] while simultaneously accounting for stronger adsorption of larger molecules;[23] see Supporting Section 5 for more details.

The critical membrane thickness increases with $X^{1/2}$, see Figure 6. Because $X^{1/2}$ increases with decreasing temperature for a given molecule (e.g. methane), surface barriers get stronger as the temperature drops. Strikingly, the enhancement of the critical membrane thickness follows more or less exactly the square root of the enhancement of the Henry coefficient (dashed line). As will be explained below, this square root correlation is caused by the functional relationship of the (free) energy and its associated residence probability in conjunction with a mean-field theory[28] based argument.

The dimensionless Henry coefficient can be written as

$$K_{\mathrm{H}} = \frac{\langle c_{\mathrm{zeol}} \rangle}{\langle c_{\mathrm{gas}} \rangle}, \tag{6}$$

where $\langle c_{\mathrm{zeol}} \rangle$ and $\langle c_{\mathrm{gas}} \rangle$ are the average concentrations in the adsorbed (zeolite) phase and in the bulk gas, respectively. Residence probabilities, P, are directly proportional to concentrations. The average concentration in the zeolite, $\langle c_{\mathrm{zeol}} \rangle$, can be approximated with the probability at the intracrystalline free-energy well (P_{zeol}) because, there, the molecules spend most time. The functional relationship between free energy and residence probability is given by $\beta F = -\ln P + \mathrm{const}$. Hence, the difference between free energy in the gas and inside the zeolite is $\beta(F_{\mathrm{gas}} - F_{\mathrm{zeol}}) \sim \ln K_{\mathrm{H}}$ (left-hand side of inset in Figure 6). Neglecting any structural details of the zeolite membrane and thus details of the free-energy profile (solid blue line in the inset), and interpolating between gas and zeolite space linearly (thick dotted line in inset), the decisive free-energy difference $\Delta\beta F^{\ddagger}$ is approximately 1/2 $\ln K_{\mathrm{H}}$ which translates to a square root dependence for the critical membrane length ($\delta_{\mathrm{crit}} \propto \exp \Delta\beta F^{\ddagger} \sim K_{\mathrm{H}}^{1/2}$). Obviously, these arguments hold only if the intracrystalline barrier is comparable to the barrier at the surface just in front of the pore mouth, i.e. the barrier experienced by gas molecules trying to enter from the bulk gas.

Discussion

Concerning the adsorbent, we can draw two main conclusions:

1. The importance of surface barriers increases with the smoothness of the nanopore, as the comparison between AFI and LTL suggests. This is supported by the work of Newsome and Sholl[2] who have investigated carbon nanotubes (extremely smooth) revealing very strong surface barriers, and by a current study by Combariza and Sastre[19]. The latter authors found virtually no surface barriers for methane uptake in a siliceous LTA slab ($\delta_{\text{crit}} \sim 1$ unit cell), the structure of which exhibits very large intracrystalline barriers (very corrugated pore wall).

2. Comparing the impact of surface barriers on the basis of our critical thickness at zero pressure and the estimate given by Combariza and Sastre,[19] a distinct trend is observable which follows the order MFI>AFI>LTL>LTA and which mirrors the order of increasing host density (MFI: 18 Si-atoms/[1000 Å^3]; AFI: 17.3; LTL: 16.3; LTA: 14.4). In fact, this provides an additional indication of the importance of the rough mean field between bulk gas and zeolite space on surface barriers, as has been discussed in the previous section.

Interestingly enough, both conclusions can, at least from a conceptual view, be exploited in regard of "material tailoring" to decrease surface barriers by choosing less smooth pores in highly porous hosts.

Although both the molecule type (alkane *vs*. alkene) and the chain length have very little impact on the strength of surface barriers, an interesting conclusion can be drawn regarding the mobile species. The bulk fluid state of the here studied hydrocarbons was gaseous. As we have shown, the more the critical pressure is approached, the more the impact of surface barriers decreases because the fluxes and thus the transport resistances in the boundary layer and in the zeolite become equal. Moreover, the predictability of the critical membrane thickness by the gas-flux model and the link between surface barriers and Henry's law provide indication that the thermodynamic state of the fluid plays an important role for surface barriers. In this context, it is interesting that Webb and Grest[29] studied liquid hexadecane entering into and traveling through a silicalite zeolite by mo-

lecular dynamics where the fluid bulk phase was liquid. The authors found that there did not exist significant surface barriers for this system because the entering mechanism of the long molecule was mainly determined by the subsurface pore structure.[29] Together with our results, we therefore conclude that surface barriers, as triggered by ideal structures, are expected to be significant for gases in contact with quite thin zeolite layers only (thickness $\lesssim$ 100 unit cells), but not for liquids and supercritical fluids.

The gained insights confirm current experimental breakthroughs by the group around Kärger and Chmelik on MOF Zn(tbip)[5,9] – a nanoporous material with a one-dimensional pore system. Combining experimental microscopy methods with statistical modeling, the group thoroughly studied the transport characteristics of guest molecules in single Zn(tbip) crystals.[5,9] The diffusion coefficients of *n*-alkanes in that MOF were extremely small – in most cases more than two magnitudes below the here probed ones. This was probably due to the very narrow windows connecting adjacent segments forming large intracrystalline diffusion barriers.[5] Most important, however, the authors reported large surface barriers whose primary nature was identified as blocked pore entrances (99.95%) and internal lattice defects, causing the extremely slow uptake. Because of the large intracrystalline barriers and the large crystal size ($>$10 μm), our study, by contrast, would have predicted no significant influence of surface barriers. Viewed from a different angle, the ideal crystal structures (no defects) and highly ideal surfaces (all channels open) from our study cannot be the reason for the surface barriers from the experimental works which clearly supports the findings of the Kärger's and Chmelik's group.

Finally, an important implication follows from our results for such an industrially relevant process as benzene alkylation. Hansen et al.[30] investigated the reaction-diffusion behavior of benzene alkylation over single H-ZSM-5 particles on the basis of a multi-scale simulation approach. Since diffusion limitation was very important,[30] the question arises whether or not surface barriers would have had a significant impact on the transport limitation and, hence, on the apparent reaction rate. Benzene and ethylbenzene exhibited very small diffusion coefficients (three magnitudes below our smallest D_S). Therefore, it seems unlikely that surface barriers would have been important for the

transport limitation of these bulky molecules. By contrast, ethene transport might potentially have been affected by surface barriers because of quite large diffusivities (10^{-8} m^2/s) and small crystal sizes (down to 0.1 μm). However, Hansen et al.[30] clearly showed that the reaction-diffusion system was hardly sensitive to orders-of-magnitude changes in the diffusion coefficient and thus transport rate of ethene. We therefore conclude that the surface barriers reported in this work would not have influenced the apparent reaction rates and thus effectiveness factors of benzene alkylation as determined by Hansen et al.[30]

Conclusions

In order to sum up we will address the questions raised in the Introduction.

1. The impact of surface barriers can be well assessed by a critical crystal length beyond which the influence can be assumed insignificant.[11]

2. The barriers strongly depend on the nanopore type and on the thermodynamic state of the surrounding fluid phase, and

3. they are triggered by the ideal crystal structure and by highly ideal surfaces.

On the basis of these insights, our study finally forecasts that surface barriers will be of importance in many cases of the evolving generation of ultra-thin, highly oriented and well intergrown zeolite films[1,3,4] because the idealized surface alone will retard the overall transport significantly – be it in the analysis of uptake/tracer-exchange experiments or in the design of membrane reactors.

Acknowledgment

We gratefully thank Jörg Kärger and Christian Chmelik for stimulating discussions. This work was supported by the German Science Foundation (Deutsche Forschungsgemeinschaft – DFG, in priority program SPP 1155).

Associated Content

Supporting Information. Methodology details, data complements, derivations, crystal structures, graphics links, list of symbols. This material is available free of charge via the Internet at http://pubs.acs.org.

References

(1) Lai, Z.; Bonilla, G.; Diaz, I.; Nery, J. G.; Sujaoti, K.; Amat, M. A.; Kokkoli, E.; Terasaki, O.; Thompson, R. W.; Tsapatsis, M.; Vlachos, D. G. *Science* **2003**, *300*, 456–460.

(2) Newsome, D. A.; Sholl, D. S. *Nano Lett.* **2006**, *6*, 2150–2153.

(3) Veziri, C. M.; Palomino, M.; Karanikolos, G. N.; Corma, A.; Kanellopoulos, N. K.; Tsapatsis, M. *Chem. Mater.* **2010**, *22*, 1492–1502.

(4) Yoo, W. C.; Stoeger, J. A.; Lee, P.-S.; Tsapatsis, M.; Stein, A. *Angew. Chem., Int. Ed.* **2010**, *49*, 8699–8703.

(5) Hibbe, F.; Chmelik, C.; Heinke, L.; Pramanik, S.; Li, J.; Ruthven, D. M.; Tzoulaki, D.; Kärger, J. *J. Am. Chem. Soc.* **2011**, *133*, 2804–2807.

(6) Chmelik, C.; Heinke, L.; Valiullin, R.; Kärger, J. *Chem. Ing. Tech.* **2010**, *82*, 779–804.

(7) Newsome, D. A.; Sholl, D. S. *J. Phys. Chem. B* **2005**, *109*, 7237–7244.

(8) Zimmermann, N. E. R.; Smit, B.; Keil, F. J. *J. Phys. Chem. C* **2010**, *114*, 300–310.

(9) Heinke, L.; Kärger, J. *Phys. Rev. Lett.* **2011**, *106*, 074501.

(10) Caro, J.; Noack, M. *Microporous Mesoporous Mater.* **2008**, *115*, 215–233.

(11) Arya, G.; Maginn, E. J.; Chang, H.-C. *J. Phys. Chem. B* **2001**, *105*, 2725–2735.

(12) Beerdsen, E.; Dubbeldam, D.; Smit, B. *Phys. Rev. Lett.* **2006**, *96*, 044501.

(13) Qiu, S.; Pang, W.; Kessler, H.; Guth, J. L. *Zeolites* **1989**, *9*, 440–444.

(14) Barrer, R. M.; Villiger, H. Z. *Z. Kristallogr.* **1969**, *128*, 352–370.

(15) van Koningsveld, H.; van Bekkum, H.; Jansen, J. C. *Acta Crystallogr., Sect. B: Struct. Sci.* **1987**, *43*, 127–132.

(16) Zimmermann, N. E. R.; Haranczyk, M.; Sharma, M.; Liu, B.; Smit, B.; Keil, F. J. *Mol. Simul.* **2011**, *37*, 986–989.

(17) Zimmermann, N. E. R.; Jakobtorweihen, S.; Beerdsen, E.; Smit, B.; Keil, F. J. *J. Phys. Chem. C* **2007**, *111*, 17370–17381.

(18) Krishna, R.; van Baten, J. M. *Microporous Mesoporous Mater.* **2011**, *137*, 83–91.

(19) Combariza, A. F.; Sastre, G. *J. Phys. Chem. C* **2011**, *115*, 13751–13758.

(20) Crank, J. *The Mathematics of Diffusion*, 2nd ed.; Oxford University Press: New York, USA, 1975.

(21) Dubbeldam, D.; Beerdsen, E.; Vlugt, T. J. H.; Smit, B. *J. Chem. Phys.* **2005**, *112*, 224712.

(22) Poling, B. E.; Prausnitz, J. M.; O'Connell, J. P. *The Properties of Gases and Liquids*; McGraw-Hill: New York, USA, 2001.

(23) Dubbeldam, D.; Calero, S.; Vlugt, T. J. H.; Krishna, R.; Maesen, T. L. M.; Smit, B. *J. Phys. Chem. B* **2004**, *108*, 12301–12313.

(24) Liu, B.; Smit, B.; Rey, F.; Valencia, S.; Calero, S. *J. Phys. Chem. C* **2008**, *112*, 2492–2498.

(25) Frenkel, D.; Smit, B. *Understanding Molecular Simulations: From Algorithms to Applications*; Academic Press: San Diego, USA, 2002.

(26) García-Pérez, E.; Schnell, S. K.; Castillo, J. M.; Calero, S.; Kjelstrup, S.; Dubbeldam, D.; Vlugt, T. J. H. *J. Phys. Chem. C* **2011**, *115*, 15355–15360.

(27) Jakobtorweihen, S.; Hansen, N.; Keil, F. J. *Mol. Phys.* **2005**, *103*, 471–489.

(28) Chandler, D. *Introdcution to Modern Statistical Mechanics*; Oxford University Press: New York, USA, 1987.

(29) Webb, E. B.; Grest, G. S. *J. Chem. Phys.* **2002**, *116*, 6311–6321.

(30) Hansen, N.; Krishna, R.; van Baten, J. M.; Bell, A. T.; Keil, F. J. *J. Phys. Chem. C* **2009**, *113*, 235–246.

Figure 1: Zeolites investigated: AFI (top), LTL (center), MFI (bottom). Free-energy profiles of methane in all three zeolites are plotted along with representations of the repetitive pore structures (center) and the two external surfaces which mark the left and right-hand borders of the single crystal slabs. The dividing surfaces for flux computation are identified as vertical lines. The free-energy wells, left and right from the barriers, are highlighted by open circles. Those mark the end points for reactive flux simulations. λ is the length of a single diffusion event inside the crystal. Black arrows indicate the direction along which the membranes were aligned.

Figure 2: Self-diffusion coefficients from two different tracer-exchange evaluation protocols as functions of membrane thickness, δ. The effective self-diffusivity, $D_{\mathrm{S,eff}}$ obtained by Eq. 1, approaches the true one, D_{S} by Eq. 2, for thick membranes only.

Figure 3: Critical membrane thickness, δ_{crit}, as a function of reduced pressure, $p^* = p/p_{\mathrm{crit}}$, for different *n*-alkanes (C1-C6) and *n*-alkenes (C1-C2) adsorbed in all-silica AFI-type zeolites (membranes were truncated at the position of the cage atoms). Note that (i) while the symbols represent *pure* simulation results, the lines are obtained by substituting $j^{\ddagger}_{\mathrm{surf}}(p^*)$ with $j_{\mathrm{gas}}(p^*)$ in Eq. (3), (ii) zero pressure corresponds to the limit where a single fluid molecule is found in the simulation box, and (iii) the lower range of the ordinate was set to the thickness of the AFI unit cell, z_{UC}.

Figure 4: Critical membrane thickness, δ_{crit}, *vs*. reduced pressure, $p^* = p/p_{\mathrm{crit}}$, for LTL (cf. Figure 3).

Figure 5: Critical membrane thickness, δ_{crit}, *vs*. reduced pressure, $p^* = p/p_{\text{crit}}$, for MFI (cf. Figure 3 and Figure 4). a) "Tight-canyon" surface (Figure 1 bottom left); b) flat surface (Figure 1 bottom right).

Figure 6: Enhancement of critical membrane thickness relative to T_{ref} with square root of dimensionless coefficient X (=change in Henry coefficient induced by temperature variation away from T_{ref}). The straight line depicts the case of one-to-one correspondence. While (c) indicates results obtained with the cage-wise truncated surface, (w) refers to the window-wise truncated surface. Inset: Representative free-energy profile (blue solid line) providing an explanatory approach to the square root dependence (thick dashed line: rough approximation to $F(q)$).

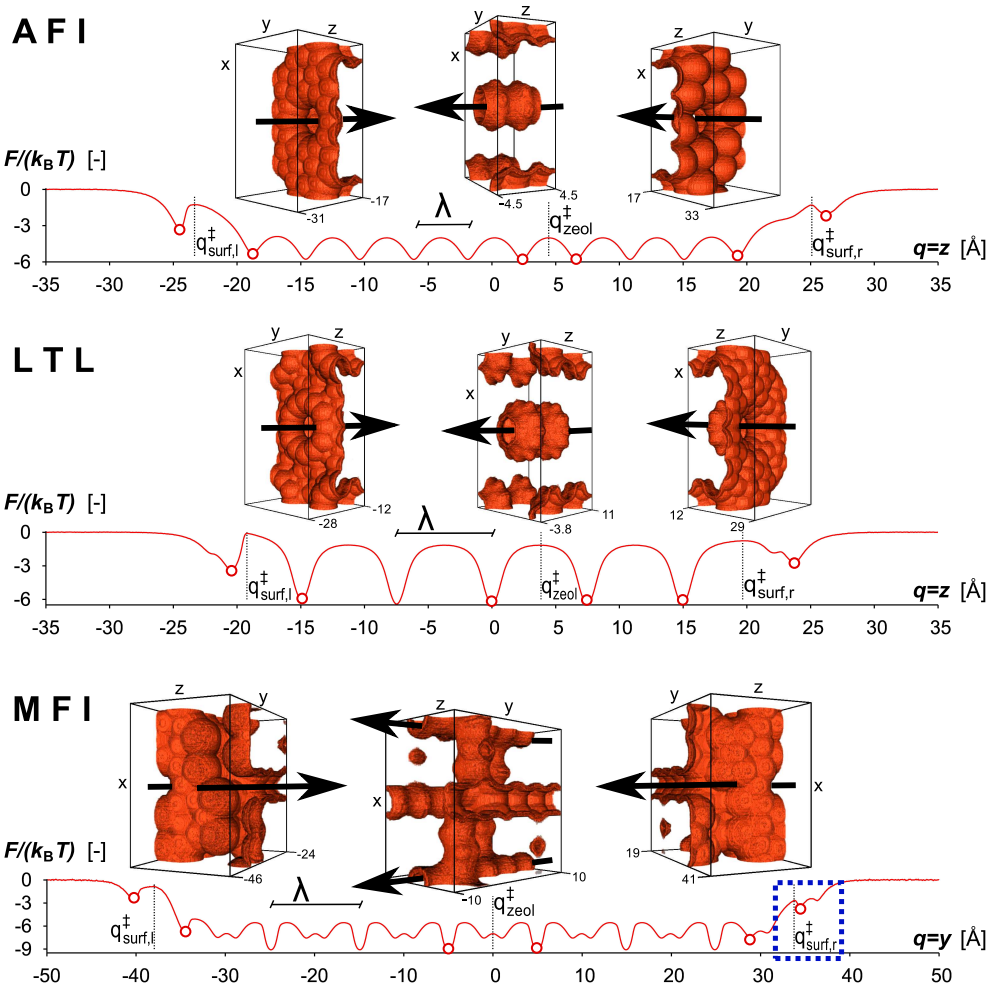
A F I
F/(k_B T) [-]
0
-3
-6
-35 -30 -25 -20 -15 -10 -5 0 5 10 15 20 25 30 35
q‡surf,l
q‡zeol
q‡surf,r
λ
q=z [Å]
L T L
F/(k_B T) [-]
0
-3
-6
-35 -30 -25 -20 -15 -10 -5 0 5 10 15 20 25 30 35
q‡surf,l
q‡zeol
q‡surf,r
λ
q=z [Å]
M F I
F/(k_B T) [-]
0
-3
-6
-9
-50 -40 -30 -20 -10 0 10 20 30 40 50
q‡surf,l
q‡zeol
q‡surf,r
λ
q=y [Å]

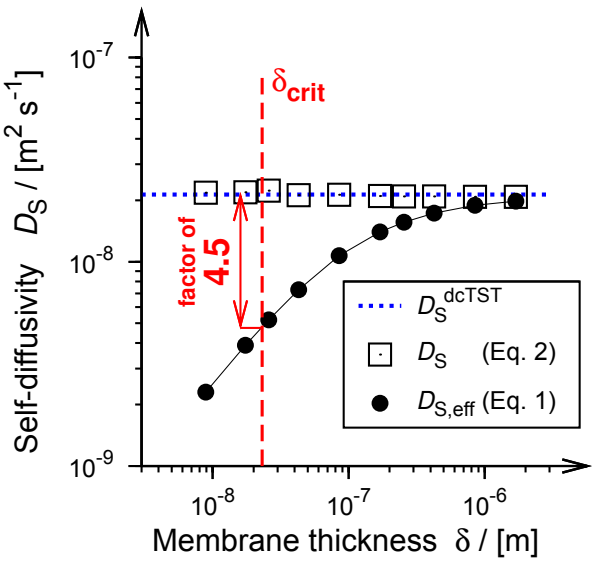
Self-diffusivity D_S / [m^2 s^{-1}]
10^{-7}
10^{-8}
10^{-9}
δ_{crit}
factor of 4.5
D_S^{dcTST}
D_S (Eq. 2)
$D_{S,eff}$ (Eq. 1)
10^{-8}
10^{-7}
10^{-6}
Membrane thickness δ / [m]

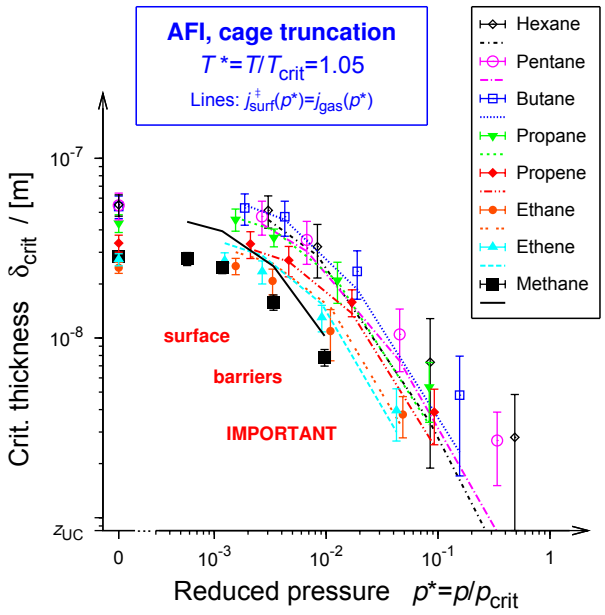
AFI, cage truncation
T*=T/T_crit=1.05
Lines: j‡surf(p*)=jgas(p*)
Hexane
Pentane
Butane
Propane
Propene
Ethane
Ethene
Methane
surface
barriers
IMPORTANT
Crit. thickness δcrit / [m]
10^-7
10^-8
zUC
0
10^-3
10^-2
10^-1
1
Reduced pressure p*=p/pcrit

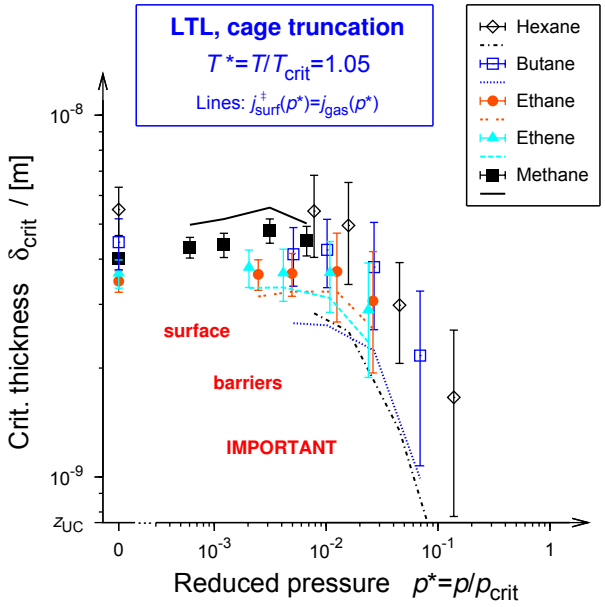
LTL, cage truncation
T*=T/T_crit=1.05
Lines: j‡surf(p*)=jgas(p*)
Hexane
Butane
Ethane
Ethene
Methane
surface
barriers
IMPORTANT
Crit. thickness δcrit / [m]
10^-8
10^-9
zUC
0
10^-3
10^-2
10^-1
1
Reduced pressure p*=p/pcrit

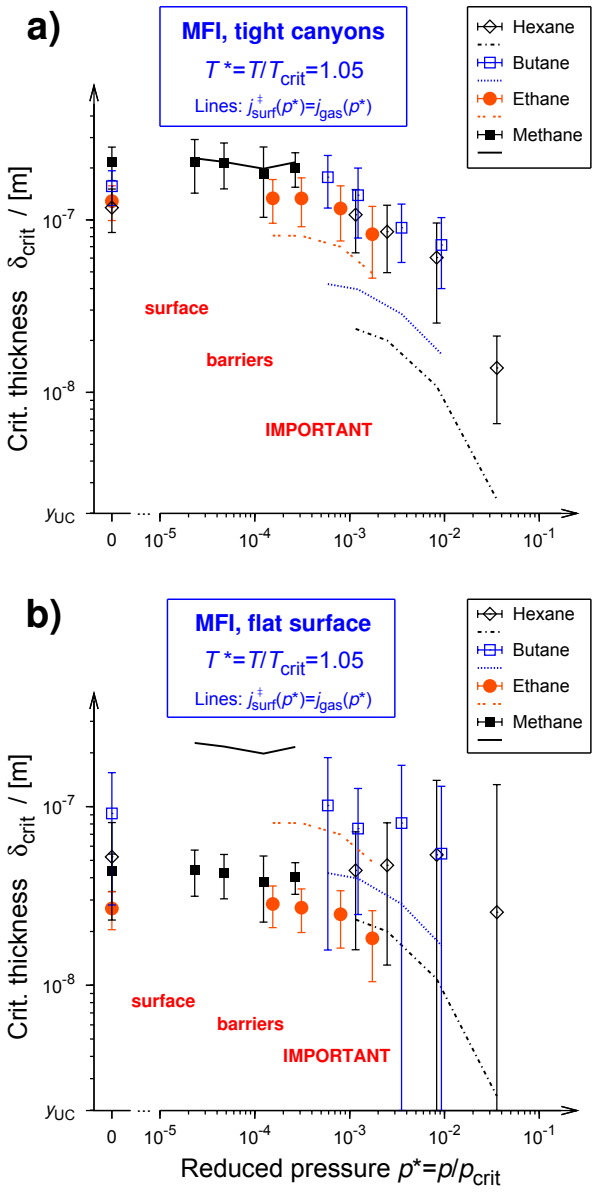
a)
MFI, tight canyons
T*=T/T_crit=1.05
Lines: j‡surf(p*)=jgas(p*)
Hexane
Butane
Ethane
Methane
surface
barriers
IMPORTANT
Crit. thickness δcrit / [m]
10^-7
10^-8
yUC
0
10^-5
10^-4
10^-3
10^-2
10^-1
b)
MFI, flat surface
T*=T/T_crit=1.05
Lines: j‡surf(p*)=jgas(p*)
Hexane
Butane
Ethane
Methane
surface
barriers
IMPORTANT
Crit. thickness δcrit / [m]
10^-7
10^-8
yUC
0
10^-5
10^-4
10^-3
10^-2
10^-1
Reduced pressure p*=p/pcrit

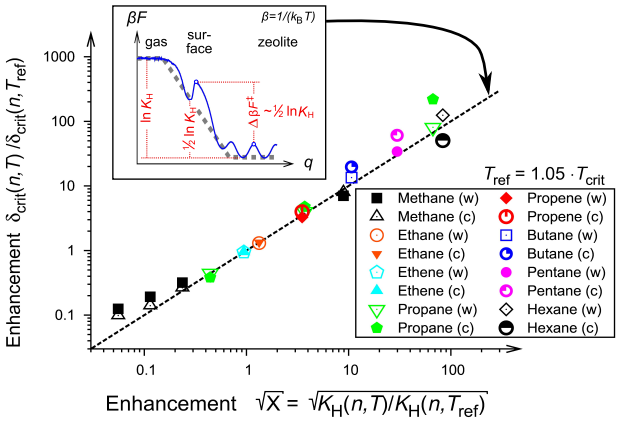
βF
β=1/(k_B T)
gas
sur-
face
zeolite
ln K_H
½ ln K_H
Δ βF‡
~½ ln K_H
q
Enhancement δ_crit(n, T) /δ_crit(n, T_ref)
1000
100
10
1
0.1
0.1
1
10
100
Enhancement √X = √K_H(n, T)/K_H(n, T_ref)
T_ref = 1.05 · T_crit
Methane (w)
Methane (c)
Ethane (w)
Ethane (c)
Ethene (w)
Ethene (c)
Propane (w)
Propane (c)
Propene (w)
Propene (c)
Butane (w)
Butane (c)
Pentane (w)
Pentane (c)
Hexane (w)
Hexane (c)